Tuning of Wavelengths: Synthesis and Photophysical Studies of Iridium Complexes and Their Applications in Organic Light Emitting Devices

Inamur R. Laskar and Teng-Ming Chen*

Department of Applied Chemistry, National Chiao Tung University, Hsinchu 30050, Taiwan

Received May 28, 2003. Revised Manuscript Received October 21, 2003

We have prepared and characterized a series of substituted 2-phenylbenzthiazole (4-CF_3, 4-Me, 4-OMe, 4-F, 4-CN, and 3-F) ligands. The intermediate di-irrido and the six-coordinated mononuclear iridium(III) dopants of the above ligands have been synthesized and characterized. These complexes are thermally stable between 275 and 300 °C depending upon the types and volatility of substituents. They emit bright yellow to orange light. The peak emission wavelengths of the dopants can be finely tuned depending upon the electronic properties of the substituents as well as their positions in the ring. In the absorption spectra, the ^{1}MLCT and ^{3}MLCT transitions have been resolved in the range of 385−450 nm. The long tail toward lower energies are assigned to ^{3}MLCT and $^3\pi-\pi^*$ transitions, which gains intensity by mixing with the higher lying ^{1}MLCT state through the spin−orbit coupling of iridium(III). All complexes exhibit one electron oxidation and the oxidation potential values can be correlated with the Hammett substituent constants. The electroluminescent characteristics for the substituted and the unsubstituted complexes have been compared and discussed.

Introduction

Luminescent d^6 metal complexes of Re(I), Ru(II), Os(II) and Ir(III) have attracted considerable attention due to their intriguing photophysical, photochemical and excited-state redox properties[1] and potential applications in photonic and photoelectronic devices.[2] Recently, there also have been growing interests in electroluminescent devices (EL) with phosphor complex dopants of the above metals as emitting layers.[3−6] Of the above phosphor emitters that have been reported for organic light-emitting diode (OLED) devices, iridium(III)-based materials have displayed the most promising due to their higher stability, larger photoluminescence efficiency and relatively shorter excited-state lifetime. The research group lead by Mark Thompson et al. has synthesized and reported a series of neutral emissive cyclometalated complexes of iridium(III)[7] and platinum(II)[8] and used them in fabrication of OLEDs successively. Researchers from Dupont de Nemours and Co. have also synthesized and characterized a series of iridium(III) complexes with fluorinated 2-arylpyridines and showed that the emissive colors of the materials can be finely tuned by systematic control of the nature and position of the substituents on the ligands.[9] The research activities inspired us to initiate a systematic study to observe the color tuning of the iridium(III) complexes by choosing a particular cyclometalated ligand with substituents exhibiting different electronic properties. Here, we choose 2-phenylbenzothiazole (bt) as the cyclometalated ligand with substituents (i.e., CF_3, F, Me, OMe, CN) showing different electronic properties to synthesize mononuclear emissive complex with iridium(III). We present the syntheses, photophysical study of $(x/ybt)_2Ir(acac)$ (x = 4CF_3, 4F, 4Me, 4OMe; y = 3F; acac = acetylacetonate), their applications in organic light emitting devices, and X-ray single-crystal structure analysis of $(CF_3bt)_2Ir(acac)$.

Experimental Section

Materials. All of the preparative work involving iridium(III) trichloride hydrate ($IrCl_3 \cdot 3H_2O$, Alfa Aesar Company

* Corresponding author. E-mail: tmchen@mail.nctu.edu.tw. Fax: 886+ 35723764.

(1) (a) Balzani, V.; Credi, A.; Scandola, F. In *Transition Metals in Supramolecular Chemistry*; Fabbrizzi, L., Poggi, A., Eds.; Kluwer: Dordrecht, The Netherlands, 1994; p 1. (b) Lehn, J.-M. *Supramolecular Chemistry—Concepts and Properties*; VCH: Weinheim, Germany, 1995. (c) Bignozzi, C. A.; Schoonover, J. R.; Scandola, F. *Prog. Inorg. Chem.* **1997**, *44*, 1.

(2) (a) Tan-Sien-Hee, L.; Mesmaeker, A. K−D. *J. Chem. Soc., Dalton Trans.* **1994**, *24*, 3651. (b) Chin, K.-F.; Cheung, K.-K.; Yip, H.-K.; Mak, T. C. W.; Che, C. M. *J. Chem. Soc., Dalton Trans.* **1995**, *4*, 657. (c) Kalyanasundaram, K.; Gratzel, M. *Coord. Chem. Rev.* **1998**, *177*, 347.

(3) (a) Lee, J. K.; Yoo, D.; Rubner, M. F. *Chem. Mater.* **1997**, *9*, 1710. (b) Gao, F. G.; Bard, A. *J. Am. Chem. Soc.* **2000**, *122*, 7426.

(4) (a) Li, Y.; Liu, Y.; Guo, J.; Wu, F.; Tian, W.; Li, B.; Wang, Y. *Synth. Met.* **2001**, *118*, 175. (b) Wang, K.; Huang, L.; Gao, L.; Jin, L.; Huang, C. *Inorg. Chem.* **2002**, *41*, 3353.

(5) Gao, F. G.; Bard, A. J. *Chem. Mater.* **2002**, *14*, 3465.

(6) (a) Lee, C.-L.; Lee, K. B.; Kim, J.-J. *Appl. Phys. Lett.* **2000**, *77*, 2280. (b) Das, R. R.; Lee C−L.; Kim J−J. *Mater. Res. Soc. Symp. Proc.* **2002**, *708*, BB3.39.1. (c) Markham, J. P. J.; Lo S.-C.; Magennis S. W.; Burn P. L.; Samuel I. D. W. *Appl. Phys. Lett.* **2002**, *80*, 2645.

(7) (a) Lamansky, S.; Djurovich, P.; Murphy, D.; Abdel-Razzaq, F.; Kwong, R.; Tsyba, I.; Bortz, M.; Mui, B.; Bau, R.; Thompson, M. E. *Inorg. Chem.* **2001**, *40*, 1704. (b) Lamansky, S.; Djurovich, P.; Murphy, D.; Abdel-Razzaq, F.; Lee, H.-F.; Adachi, C.; Burrows, P. E.; Forrest, S. R.; Thompson, M. E. *J. Am. Chem. Soc.* **2001**, *123*, 4304. (c) Thompson, M. E.; Lamansky, S.; Djurovich, P.; Murphy, D.; Abdel-Razzaq, F.; Kwong, R.; Forrest, S. R.; Baldo, M. A.; Burrows, P. E. U.S. Patent 20020034656A1.

(8) Brooks, J.; Babayan, Y.; Lamansky, S.; Djurovich, P. I.; Tsyba, I.; Bau, R.; Thompson, M. E. *Inorg. Chem.* **2002**, *41*, 3055.

(9) Grushin V. V.; Herron, N.; LeCloux, D. D.; Marshall, W. J.; Petrov, V. A.; Wang, Y. *Chem. Commun.* **2001**, 1494.

10.1021/cm030410x CCC: $27.50
Published on Web 12/02/2003

Ltd.), 2-ethoxyethanol ($H_5C_2OC_2H_4OH$, Fluka), and all other reagents (Tokyo Chemical Industry, Japan) were carried out in an inert atmosphere and used without further purification.

Optical Measurements and Compositions Analysis. The ultraviolet−visible (UV−vis) spectra of the phosphorescent Ir(III) complexes were measured on an UV−vis spectrophotometer (Agilent model 8453) and corrected for background due to solvent absorption. Photoluminescence (PL) spectra were carried out with a spectrophotometer (Jobin-Yvon Spex, model Fluorolog-3). Comparative quantum efficiencies have been measured using spectra ARC sense analysis, v 1.08 software and $(bt)_2Ir(acac)$ as a reference. NMR spectra were recorded on Varian 300 MHz. MS spectra (EI and FAB) were taken by micromass TRIO-2000. Elemental analyses have been carried out by using a Heraeus CHN-O-RAPID analyzer. Cyclic voltammetry (CV) analyses were performed by using CHI 2.05 and the TG-DTA analysis was carried out by using a thermal analyzer (SEIKO 1TG/DTA 200).

Crystallography. Single-crystal diffraction data for $(CF_3$-$bt)_2Ir(acac)$ were collected on a Bruker CCD diffractometer equipped with a normal focus, 3-kW sealed-tube X-ray source (λ = 0.71073). Data collection in the ω scan mode (width of 0.3°/frame), cell refinement and data reduction were carried out using the program Bruker SHELXTL.[10] The structure was solved by direct methods using the SHELXTL version 5.1 software packages.[10] The structure was refined by full-matrix least-squares methods based on F^2 using SHELXTL version 5.1.[10] The non-hydrogen atom positions were refined anisotropically, whereas the hydrogen positions were not refined.

Syntheses. Synthesis of x/ybt (x = $4CF_3$, 4F, 4Me, 4OMe, 4-CN and y = 3F; bt = (2-phenyl)benzothiazole): These were prepared via a general method[11] where 10 mmol of *o*-aminothiophenol was dissolved into 20 mL of 1-methyl-pyrrolidinone under an inert atmosphere; then the stoichiometric amount of the corresponding acid chloride was added slowly at room temperature. The mixture was heated at 100 °C for 1 h. After cooling, the solution was poured into cold water and the mixture was adjusted to pH 8−9 with 7 N aqueous ammonia. A white-colored solid compound was separated out and the crude material was filtered, washed with water several times, and further purified by column chromatography.

bt. 2-phenylbenzothiazole (yield 92%). ^{1}H NMR (300 MHz, $CDCl_3$): δ 7.86 (m, 3H), 7.64 (d, 8.1, 1H), 7.25 (m, 4H), 7.13 (m, 1H). EIMS: *m*/*z* 211, calcd 211.

(4-MeO)bt. (4-methoxy)2-phenylbenzothiazole (yield 95%). ^{1}H NMR (300 MHz, $CDCl_3$): δ 8.04 (m, 4H), 7.45 (m, 2H), 7.11 (m, 2H), 3.83 (s, 3H). EIMS: *m*/*z* 241, calcd 241.

(4-CF_3)bt. (4-trifluoromethyl)2-phenylbenzothiazole (yield 84%). ^{1}H NMR (300 MHz, $CDCl_3$): δ 8.21 (d, 2H, J = 7.8 Hz), 8.11 (d, 1H, J = 7.8 Hz), 7.94 (d, 1H, J = 7.2, Hz), 7.76 (d, 2H, J = 8.1 Hz), 7.53 (td, 1H, J = 1.2, 8.1 Hz), 7.43 (d, 1H, J = 0.9, 8.1 Hz). EIMS: *m*/*z* 279, calcd 279.

(4-Me)bt. (4-methyl)2-phenylbenzothiazole (yield 82%). ^{1}H NMR (300 MHz, $CDCl_3$): δ 8.05 (d, 1H, J 8.4 Hz), 7.98 (d, 2H, J = 8.4 Hz), 7.88 (dd, 1H, J = 0.6, 8.1 Hz), 7.47 (t, 1H, J = 7.5 Hz), 7.36 (t, 1H, J = 7.2 Hz), 7.27 (d, 2H, J = 7.8 Hz), 2.40 (s, 3H). EIMS: *m*/*z* 225, calcd 225.

(4-CN)bt. (4-cyano)2-phenylbenzothiazole (yield 90%). ^{1}H NMR (300 MHz, $CDCl_3$): δ 8.21 (dd, 2H, J = 8.7, 1.8 Hz), 8.12 (d, 1H, J = 8.7 Hz), 7.95 (dd, 1H, J = 7.8, 0.6 Hz), 7.74 (dd, 2H, J = 6.9, 2.1 Hz), 7.55 (td, 1H, J = 7.2, 1.5 Hz), 7.45 (d, 1H, J = 1.2, 8.1 Hz). EIMS: *m*/*z* 236, calcd 236.

(4-F)bt. (4-fluoro)2-phenylbenzothiazole (yield 92%). ^{1}H NMR (300 MHz, $CDCl_3$): δ 8.08 (m, 3H), 7.90 (d, 1H, J = 8.4 Hz), 7.50 (td, 1H, J = 7.2, 1.2 Hz), 7.39 (dd, 1H, J = 8.1, 1.2 Hz), 7.19 (m, 2H). EIMS: *m*/*z* 229, calcd 229.

(3-F)bt. (3-fluoro)2-phenylbenzothiazole (yield 90%). ^{1}H NMR (300 MHz, $CDCl_3$): δ 8.08 (d, 1H, J = 7.5), 7.91 (d, 1H, J = 7.8 Hz), 7.84 (m, 1H), 7.50 (m, 2H), 7.42 (m, 2H), 7.19 (m, 1H). EIMS: *m*/*z* 229, calcd 229.

Syntheses of the Dichloro-Bridged Iridium(III) Complexes, x/ybt$_2$Ir(μ-Cl)$_2$x/ybt$_2$. These were prepared[7] by refluxing the mixture of $IrCl_3 \cdot 3H_2O$ (1 mmol) and the ligands (x/ybt) (2.4 mmol) in 2-ethoxyethanol for 24−25 h. The orange-yellow mixtures were cooled to room temperature and 20 mL of 1 M HCl was added to precipitate the product. The mixture was filtered and washed with 100 mL of 1 M HCl followed by 50 mL of methanol solution several times and then dried.

[Ir(bt)$_2$Cl]$_2$. Yield 65%. (Found: C, 48.0; H, 2.1; N, 3.8. Calcd for $C_{52}H_{32}Cl_2N_4S_4Ir_2$: C, 48.2; H, 2.5; N, 4.3%). ^{1}H NMR (300 MHz, $CDCl_3$): δ 8.30 (d, 4H, J = 7.5 Hz), 7.65 (m, 16H), 6.79 (m, 12H). FABMS: *m*/*z* 1295, calcd 1295.

[Ir(4-CF_3bt)$_2$Cl]$_2$. Yield 67%. (Found: C, 42.5; H, 1.8; N, 3.3. Calcd for $C_{56}H_{28}Cl_2F_{12}N_4S_4Ir_2$: C, 42.9; H, 1.8; N, 3.6%). ^{1}H NMR (300 MHz, $CDCl_3$): δ 8.59 (dd, 4H, J = 0.75, 7.5 Hz), 7.64 (d, 4H, J = 8.1 Hz), 7.49 (dd, 4H, J = 1.2, 7.8 Hz), 7.13 (m, 12H), 6.19 (s, 4H). FABMS: *m*/*z* 1567; calcd 1567.

[Ir(4-Fbt)$_2$Cl]$_2$. Yield 61%. (Found: C, 45.3; H, 2.1; N, 3.9. Calcd for $C_{52}H_{28}Cl_2F_4N_4S_4Ir_2$: C, 45.6; H, 2.1; N, 4.0%). ^{1}H NMR (300 MHz, $CDCl_3$): δ 8.66 (dd, 4H, J = 3.0, 6.9 Hz), 7.56 (m, 4H), 7.41 (d, 4H, J = 1.2, 7.2 Hz), 7.08 (m, 8H), 6.54 (m, 4H), 5.59 (dd, 4H, J = 2.4, 10.2 Hz). FABMS: *m*/*z* 1367, calcd 1367.

[Ir(4-Mebt)$_2$Cl]$_2$. Yield 70%. (Found: C, 45.4; H, 3.0; N, 3.8. Calcd for $C_{56}H_{40}Cl_2N_4S_4Ir_2$: C, 45.6; H, 3.0; N, 4.1%). ^{1}H NMR (300 MHz, $CDCl_3$): δ 8.70 (m, 4H), 7.38 (m, 8H), 7.03 (m, 8H), 6.56 (d, 4H, J = 7.5 Hz), 5.81 (s, 4H), 1.77 (s, 12 H). FABMS: *m*/*z* 1351, calcd 1351.

[Ir(4-MeObt)$_2$Cl]$_2$. Yield 65%. (Found: C, 47.2; H, 3.1; N, 3.8. Calcd for $C_{56}H_{40}Cl_2N_4O_4S_4Ir_2$: C, 47.5; H, 3.1; N, 4.0%). ^{1}H NMR (300 MHz, $CDCl_3$): δ 8.74 (t, 4H, J = 1.8, 7.8 Hz), 7.46 (d, 4H, J = 8.4 Hz), 7.35 (dd, 4H, J = 2.1, 6.9 Hz), 7.00 (m, 8H), 6.35 (dd, 4H, J = 2.4, 8.4 Hz), 5.55 (d, 4H, J = 2.4 Hz), 3.03 (s, 12H). FABMS: *m*/*z* 1414, calcd 1415.

[Ir(3-Fbt)$_2$Cl$_2$]$_2$. Yield 61%. (Found: C, 45.4; H, 2.1; N, 3.7. Calcd for $C_{52}H_{28}Cl_2F_4N_4S_4Ir_2$: C, 45.6; H, 2.1; N, 4.0%). ^{1}H NMR (300 MHz, $CDCl_3$): δ 8.58 (m, 4H), 7.38 (m, 4H), 7.09 (m, 8H), 6.91 (m, 4H), 6.04 (m, 8H). FABMS: *m*/*z* 1367, calcd 1367.

Syntheses of (x/ybt)$_2$Ir(acac).[7] The chloride-bridged dimer, x/ybt$_2$Ir(μ-Cl)$_2$x/ybt$_2$ (0.1 mmol), acetylacetone (0.3 mmol), and sodium carbonate (1 mmol) were mixed in 10 mL of 2-ethoxyethanol (30 mL). The mixture was refluxed under nitrogen for 11−12 h. Then the reaction was cooled and the precipitate filtered. The product was purified by recrystallization from a solution of the mixture of dichloromethane and methanol (2:1).

Ir(bt)$_2$(acac), 1. Yield 90%. (Found: C, 52.1; H, 3.1; N, 3.8. Calcd for $C_{31}H_{23}N_2O_2S_2Ir$: C, 52.3; H, 3.2; N, 3.9%). ^{1}H NMR (300 MHz, DMSO-d^6): δ 8.25 (d, 2H), 7.93 (m, 2H), 7.74 (dd, 2H, J = 8.1, 1.9 Hz), 7.56 (m, 4H), 6.86 (td, 2H, J = 7.8, 1.1 Hz), 6.59 (td, 2H, J = 7.5, 1.0 Hz), 6.2 (d, 2H, 7.5 Hz), 5.12 (s, 1H), 1.71 (s, 6H). FABMS: *m*/*z* 711, calcd 711.

Ir(4-CF_3bt)$_2$(acac), 2. Yield 81%. (Found: C, 46.5; H, 2.5; N, 3.1. Calcd for $C_{33}H_{21}F_6N_2O_2S_2Ir$: C, 46.7; H, 2.5; N, 3.3%). ^{1}H NMR (300 MHz, $CDCl_3$): δ 8.06 (d, 2H, J = 8.1 Hz), 7.96 (d, 2H, J = 8.7 Hz), 7.74 (d, 2H, J = 8.1 Hz), 7.49 (m, 4H), 7.12 (d, 2H, J = 7.8 Hz), 659 (s, 2H), 5.13 (s, 1H), 1.78 (s, 6H). FABMS: *m*/*z* 847, calcd 847.

Ir(4-Fbt)$_2$(acac), 3. Yield 85%. (Found: C, 49.7; H, 2.7; N, 3.5. Calcd for $C_{31}H_{21}F_2N_2O_2S_2Ir$: C, 49.8; H, 2.8; N, 3.7%). ^{1}H NMR (300 MHz, $CDCl_3$): δ 8.02 (m, 2H), 7.90 (m, 2H), 7.65 (m, 2H), 7.44 (m, 4H), 6.60 (m, 2H), 659 (dd, 2H, J = 9.9, 2.4), 1.78 (s, 6H). FABMS: *m*/*z* 747, calcd 747.

Ir(4-Mebt)$_2$(acac), 4. Yield 86%. (Found: C, 51.2; H, 3.5; N 3.6. Calcd for $C_{33}H_{27}N_2O_2S_2Ir$: C, 53.6; H, 3.7; N, 3.8%). ^{1}H NMR (300 MHz, $CDCl_3$): δ 8.03 (d, 2H, J = 3.6 Hz), 7.87 (d, 2H, J = 5.7 Hz), 7.55 (d, 2H, J = 7.8 Hz), 7.41 (dd, 4H, J = 3.0, 5.7 Hz), 6.68 (d, 2H, J = 7.8 Hz), 6.23 (s, 2H), 5.11 (s, 1H), 2.02 (s, 6H), 1.75 (s, 6H). FABMS: *m*/*z* 739, calcd 739.

Ir(4-MeObt)$_2$(acac), 5. Yield 88%. (Found: C, 51.2; H, 3.5; N, 3.5. Calcd for $C_{33}H_{27}N_2O_4S_2Ir$: C, 51.4; H, 3.5; N, 3.6%). ^{1}H NMR (300 MHz, $CDCl_3$): δ 8.03 (d, 2H, J = 9.0 Hz), 7.83 (d, 2H, J = 8.4 Hz), 7.58 (d, 2H, J = 8.4 Hz), 7.38 (m, 4H), 6.44

(10) G. M. Sheldrick, *SHELXTL Programs*, version 5.1; Bruker AXS GmbH: Karlsruhe Germany, 1998.

(11) Brembilla, A.; Roizard, D.; Lochon, P. *Synth. Commun.* **1990**, *20*, 3379.

(dd, 2H, J = 1.8, 8.4 Hz), 5.90 (d, 2H, J = 2.4 Hz), 5.14 (s, 1H), 3.41 (s, 6H), 1.77 (s, 6H). FABMS: m/z 771, calcd 771.

Ir(3-Fbt)$_2$(acac), 6. Yield 85%. (Found: C, 49.6; H, 2.8; N, 3.5. Calcd for $C_{31}H_{21}F_2N_2O_2S_2Ir$: C, 49.8; H, 2.8; N, 3.7%). ^{1}H NMR (300 MHz, $CDCl_3$): δ 8.06 (m, 2H), 7.89 (m, 2H), 7.57 (d, 2H, J = 7.5), 7.44 (m, 2H), 6.90 (m, 2H), 6.45 (m, 2H), 6.33 (m, 2H), 5.15 (m, 1H), 1.77 (s, 6H). FABMS: m/z 747, calcd 747.

OLED Fabrication and Testing. Organic layers were fabricated by high-vacuum thermal evaporation onto a glass substrate precoated with an indium tin oxide (ITO) layer with a sheet resistance of 20 Ω. Prior to use, the ITO surface was ultrasonicated in a detergent solution followed by rinsing with deionized (DI) water, dipped into acetone, trichloroethylene, and 2-propanol, and then degreased with a vapor of 2-propanol. After degreasing, the substrate was oxidized and cleaned in a UV-ozone chamber before it was loaded into an evaporator. In a vacuum chamber at a pressure of 10^{-6} Torr, 500 Å of NPB as the hole transporting layer, 200 Å of the complex doped (7%) CBP as the emitting layer, 100 Å of 2,9-dimethyl-4,7-diphenyl-1,10-phenanthroline (BCP) as a hole and exciton blocking layer (HBL), 650 Å of Alq_3 as the electron transporting layer, and a cathode composed of 10 Å of lithium fluoride and 2000 Å of aluminum were sequentially deposited onto the substrate to give the device structure. The current−voltage ($I-V$) profiles and light intensity characteristics for the above-fabricated devices were measured in a vacuum chamber of 10^{-6} Torr at ambient temperature using a Keithley 2400 Source Meter/2000 Multimeter coupled to a PR 650 Optical Meter.

Results and Discussion

Synthesis and Characterization of (x/ybt)$_2$Ir(acac) Complexes. (x/ybt)$_2$Ir(acac) have been prepared[7] with all the substituted cyclometalated ligand, except cyano containing ligand. We have tried to synthesize the dinuclear complexes with the corresponding cyano-substituted ligand several times, but failed. The synthetic method used to prepare these complexes involves two steps. In the first step, $IrCl_3 \cdot 3H_2O$ was allowed to react with an excess of the cyclometalated ligand (2.5 times) to give a chloride-bridged dinuclear complex, i.e., (x/ybt)$_2$Ir$_2$(μ-Cl)$_2$(x/ybt)$_2$. The NMR spectra of these complexes are consistent with the heterocyclic rings of the x/ybt ligands being in a trans disposition. The chloride-bridged dinuclear complexes can be readily converted to emissive, mononuclear complexes (x/ybt)$_2$Ir(acac) by replacing the two bridging chlorides with bidentate acetylacetonate. These reactions result in (x/ybt)$_2$Ir(acac) with a yield of 85−90%. Single-crystal X-ray crystallographic studies have been carried out for one of the phosphorescent complexes, (CF$_3$bt)$_2$Ir(acac) (acac = acetylacetonate). The iridium(III) ion is octahedrally coordinated by the three chelating ligands. The coordination geometry of the "(x/ybt)$_2$Ir" fragment in the mononuclear complex is the same as that for the dinuclear complexes. All the mononuclear complex dopants are thermally stable up to 280−320 °C. The monomeric complexes can be sublimed easily at reduced pressure. ^{1}H NMR data for the ligands and dinuclear and mononuclear complexes fall in the ranges of 7.1−8.2, 5.5−8.8, and 5.9−8.2, respectively. The resonance spectra of ligands show poorly resolved multiplets, whereas the well-resolved multiplets are observed for the complexes. The maximum high-field chemical shift is observed for the proton to the ortho-metalated carbon atom that experiences the largest shielding of any of the ligand protons. Again the chemical shift of this particular proton varies with the electronic properties of the substituents present in the ligand. The complex containing CF_3-substituted ligand shows the lowest field chemical shift (i.e., 6.2 ppm) for the proton to the ortho-metalated carbon atom due to the less shielding power arising from the strong electron withdrawing property of the substituent, whereas the strongest electron releasing substituent (i.e., $-OCH_3$ group) shows the highest field chemical shift (i.e., 5.5 ppm) for the same proton.

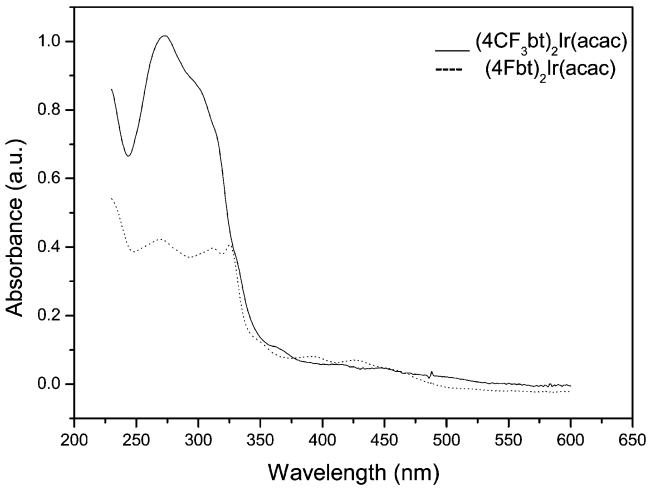

Figure 1. Absorption spectra for 1×10^{-4} M of [(4-CF$_3$bt)$_2$Ir(acac)] and [(4-Fbt)$_2$Ir(acac)] complexes in CH_2Cl_2.

Absorption Spectra. Figure 1 shows the absorption bands of **1** and **5** as a representative of the series of complexes. It suggests that the bands can be classified in two types: intense bands are observed in the ultraviolet part of the spectrum (250−350 nm) that can be assigned to the allowed ligand-centered ($\pi-\pi^*$) transitions,[7a] somewhat weaker bands are observed in the lower part of energy (λ_{max} > 385 nm). The band position, size, and the extinction coefficients suggest that these are MLCT transitions.[6b,7a,12] ^{1}MLCT and ^{3}MLCT transitions have been resolved in the range of 385−450 nm, as indicated in Table 1. Absorption in the range of 385−405 nm for all the complexes corresponds to the transition to the ^{1}MLCT state as evident from its extinction coefficient of the order 10^3. The long tail toward lower energy is assigned to ^{3}MLCT transitions and gains intensity by mixing with the higher lying ^{1}MLCT transition through the spin−orbit coupling of iridium(III).[13] This mixing is strong enough in these complexes that the formally spin forbidden ^{3}MLCT has an extinction coefficient that is almost equal to the spin allowed ^{1}MLCT transition. The presence of another transition around 360 nm of the complexes is also well pronounced, which corresponds to an admixture of MLCT and ligand $\pi-\pi^*$ states.

Ligand Tuning of Emission Wavelengths. All of these complexes (e.g., **1**−**5**) show strong luminescence both in the solid state and in organic solutions from their triplet state.[7] The maximum emission peak was found to be dependent on the polarity of the solvent, which suggests the MLCT character of the emissive state. The presence of vibrational progression in the PL spectra (Figure 2) and significant Stokes shifts (i.e.,

(12) Colombo, M. G.; Güdel, H. U. *Inorg. Chem.* **1993**, *32*, 3081.
(13) Lever, A. B. P. *Inorganic Electronic Chemistry* (second edition); Elsevier: New York, 1984; p 117.

Table 1. Photophysical and Electrochemical Data for (x/ybt)$_2$Ir(acac) Complexes

complex (X−subs)	absorbance λ (log ϵ)	emission λ_{max} (nm) CH_2Cl_2	quantum yield (.xIr-bt)	ΔE (ev)	ox. pot. V vs calm	Hamett. subs. const. $\sigma = (\sigma_R + \sigma_I)$
1 pristine	408 (3.7); 447 (3.7)	560	1.0	2.3	1.035	
2 (−4CF_3)	401 (3.8); 451 (3.7)	567	1.8	2.2	1.405	0.54
3 (−4F)	390 (3.9); 427 (3.9)	544	1.1	2.4	1.277	0.11
4 (−4Me)	394 (3.9); 440 (3.9)	559	2.0	2.3	1.151	−0.17
5 (−4OMe)	387 (4.3); 424 (4.1)	544	2.2	2.4	1.043	−0.24
6 (−3F)	391 (3.9); 438 (3.8)	555	3.1	2.3	1.338	

110−125 nm) assists us in assigning the $^3\pi-\pi^*$ states as the dominant emitting state at room temperature in equilibrium with the other neighboring states. Typically, on changing the types of substituents (i.e., CF_3, Me, F, and OMe) in (2-phenyl)benzothiazole, we have observed a marked effect on systematic shifting of the maximum emission peak of (x/ybt)$_2$Ir(acac) complexes, as indicated by the solution photoluminescence spectra represented in Figure 2. As summarized in Table 1, among the various substituted complexes, the strongest electron withdrawing trifluoromethyl group and its complex **2** were found to exhibit the emission wavelength (λ_{em}) much longer than that of the complex containing unsubstituted one, whereas the methoxy and fluoro groups containing complexes (i.e., **5** and **3**) exhibit the maximum emission wavelength (Table 1) shorter than the unsubstituted complex, **1** having the predominating factor π-donation. On changing the position of the substituents (i.e., 4F → 3F), the maximum emission peak of the complex shows the large bathochromic shift and the shape of the emission curve (Figure 3) is also quite different. 4F-substituted complex (**3**) shows a narrow and structure type transition, whereas the 3F-substituted complex (**6**) exhibits a broad and featureless transition. It has been shown that the maximum emission peak wavelength of the complexes can be tuned by ∼35 nm depending on the electronic nature of the substituents (Figure 2). Figure 4 shows the intensity of the solution luminescence of various complexes with respect to the nature of the substituents. The quantum efficiencies have been compared of the various complexes with respect to the unsubstituted one, **1** (Table 1). We have observed that the quantum efficiency is increased for all the substituted complexes, with the maximum value appearing in the complex, **6**. The HOMO/LUMO energy has also been calculated for all the complexes (Table 1) based on the experimental redox potential value and the absorbance wavelength. It is observed that the energy gap (HOMO−LUMO) for the trifluoromethyl-substituted complex, **2** is the least, whereas 4-OMe and 3-F substituted complexes show the maximum energy gap and the rest exhibit intermediate values among all investigated. Trifluoromethyl-substituted complex shows emission at the maximum wavelength and 4-OMe and 3F-substituted complexes exhibit minimum emission wavelength that can be correlated to the HOMO−LUMO energy gap of the complexes (Table 1).

Redox Chemistry. Analysis by cyclic voltammetry shows that the (x/ybt)$_2$Ir(acac) complexes all undergo a reversible one-electron oxidation; however, no reduction processes were observed in dichloromethane. The de-

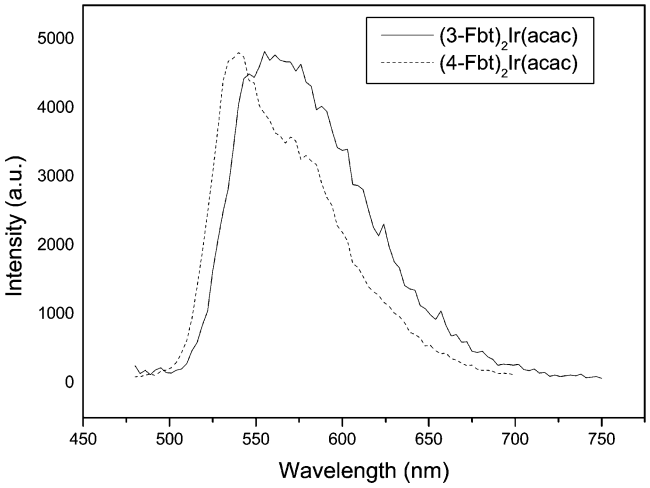

Figure 3. Solution photoluminescence spectra of [(3-Fbt)$_2$Ir-(acac)] and [(4-Fbt)$_2$Ir(acac)] complexes.

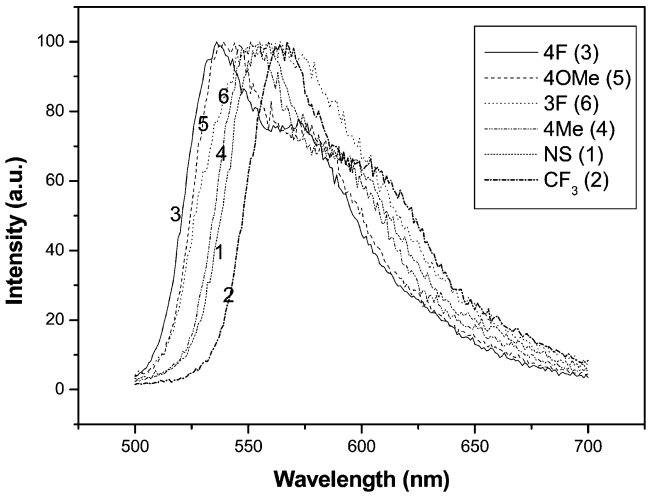

Figure 2. Normalized solution photoluminescence spectra for 1×10^{-4} M of [(x/ybt)$_2$Ir(acac)] complexes in CH_2Cl_2.

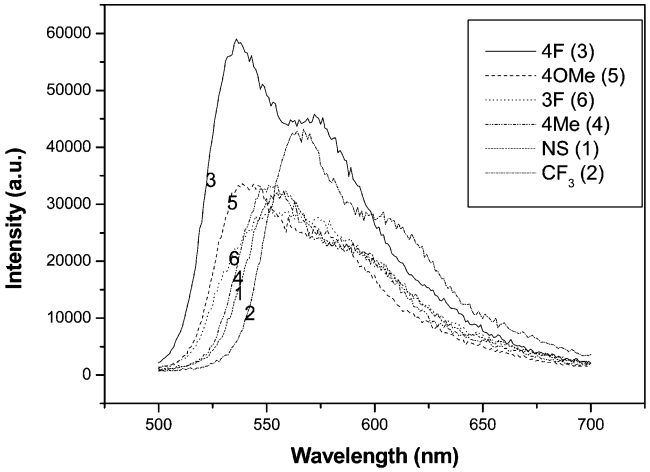

Figure 4. Solution photoluminescence spectra for 1×10^{-4} M of [(x/ybt)$_2$Ir(acac)] complexes in CH_2Cl_2.

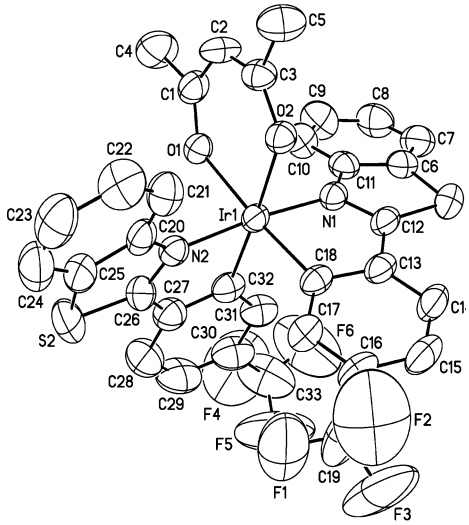

Figure 5. ORTEP drawing of [(4-CF_3bt)$_2$Ir(acac)]; the thermal ellipsoids represent 50% probability limit.

creasing order of oxidation potential of the complexes has been observed in the following: **2** (4-CF_3bt) > **3** (4-Fbt) > **4** (4-Mebt) > **5** (4-OCH_3bt) (Table 1). This observation can be rationalized in terms of the Hammett substituent constant σ, which is a characteristic of the electronic effect of a substituent. Electron-withdrawing substituents exhibit positive σ values and electron-donating groups have negative values. The magnitude of σ also varies according to its position on the aryl ring relative to the reactive site. Values for Hammett substituent constants ($\sigma = \sigma_R + \sigma_I$) for the substituents such as $-CF_3$, $-F$, $-Me$, and $-OMe$ are given in Table 1. σ_R and σ_I ($\sigma_R = \sigma_m - \sigma_p$; $\sigma_I = \sigma_m$) are the electronic factors for the substituents operated through resonance and inductive effects, respectively. The order of the positive value of σ (Table 1) has been found as the following: **2** ($-CF_3$) > **3** ($-F$) > **4** ($-Me$) > **5** ($-OMe$), which shows the order of the strength of the electron withdrawing nature of the substituents in the complexes and, conversely, it is the increasing order of oxidation potentials (Table 1).

Description of the Structure of $(CF_3bt)_2Ir(acac)$, 2. The crystal structure of the complex **2** is represented with an ORTEP diagram in Figure 5. Crystallographic data are also given in Table 2, and selected bond lengths and bond angles are presented in Table 3. The complex exhibits an octahedral coordination geometry around Ir and prefers *cis*-C,C *trans*-N,N chelate disposition instead of *trans*-C,C *trans*-N,N chelate. Electron-rich σ-phenyl ligands normally exhibit very strong trans influence and trans effect. Therefore, the trans C−C arrangement is expected to be higher in energy (thermodynamics) and thus more labile (kinetics). This well-known phenomenon has been recently referred to as "transphobia".[14] The Ir−C bonds of these complexes (Ir−C_{av} = 1.992(6) Å) are found to be shorter than the Ir−N bonds (Ir−N_{av} = 2.053(5) Å). The Ir−C bond length is similar to those in the analogous complexes reported.[15−17] Furthermore, the Ir−N bond lengths also fall within the range of values for those of the similar type of reported complexes.[15−17] The Ir−O bond lengths of 2.131(4) and 2.138(4) Å are longer than the mean Ir−O bond length of 2.088 Å reported and these observations reflect the large trans influence of the phenyl groups. All other bond lengths and bond angles within the chelate ligands are analogous to the similar type of complexes.[15−17]

Table 2. Crystal Data and Structure Refinement for $(CF_3Bt)_2Ir(acac)$

empirical formula	$C_{33}H_{21}F_6IrN_2O_2S_2$
formula weight	847.84
temperature	295(2) K
wavelength	0.71073 Å
crystal system	orthorhombic
space group	*Pbca*
unit cell dimensions	a = 12.5646(6) Å b = 17.9936(9) Å c = 27.8150(14) Å
volume	6288.5(5) Å^3
Z	8
density (calculated)	1.791 mg/m^3
absorption coefficient	4.449 mm^{-1}
F(000)	3296
crystal size	0.40 × 0.30 × 0.10 mm^3
θ range for data collection	1.46 to 28.29°.
index ranges	$-16 \le h \le 16$ $-18 \le k \le 23$ $-36 \le l \le 37$
reflections collected	37577
independent reflections	7633 [R(int) = 0.0523]
absorption correction	empirical
max. and min. transmission	0.95767 and 0.50780
refinement method	full-matrix least-squares on F^2
data/restraints/parameters	7633/0/415
goodness-of-fit on F^2	1.082
final R indices [$I > 2\sigma(I)$]	R1 = 0.0488, wR2 = 0.0856
R indices (all data)	R1 = 0.0876, wR2 = 0.0969
largest diff. peak and hole	1.089 and −1.707 e Å^{-3}

Table 3. Selected Bond Distancess [Å] for $(CF_3Bt)_2Ir(acac)$

atom(1)−atom (2)	distance (Å)
Ir(1)−C(32)	1.989(6)
Ir(1)−C(18)	1.994(6)
Ir(1)−N(1)	2.049(5)
Ir(1)−N(2)	2.056(5)
Ir(1)−O(2)	2.131(4)
Ir(1)−O(1)	2.138(4)

In addition, thermal ellipsoid values for the atoms C19, C33, and F1−F6 are exceptionally high, which suggests the severe steric interaction between the substituents, trifluoromethyl between two separate ligands.

Description of OLED Devices Prepared with $(CF_3bt/bt)_2Ir(acac)$ Dopants in an Emissive Layer. We have also fabricated two electroluminescent (EL) devices using one of the substituted complexes, (CF_3-bt)$_2$Ir(acac) (device **a**) and the unsubstituted complex (device **b**) as dopants in the emitting layer. To compare the relative electroluminescent properties, the device structure and the thickness of the layers (i.e., ITO/NPB (500 Å)/ CBP + 7% dopant (200 Å)/BCP (100 Å)/Alq_3-(650 Å)/LiF(10 Å)/Al(2000 Å)) have been kept constant. The phosphors were then doped into the emissive layer of the OLED at a concentration of 7%. The comparative variation of quantum efficiency as a function of current density for the devices **a** and **b** are shown in Figure 6.

(14) Vicente J.; Arcas, A.; Bautista, D.; Arellano, M. C. R. de *J. Organomet. Chem.* **2002**, *663*, 164.

(15) Garces, F. O.; Dedian, K.; Keder, N. L.; Watts, R. J. *Acta Crystallogr.* **1993**, *C49*, 1117.

(16) Urban, R.; Krämer, R.; Mihan, S.; Polborn, K.; Wagner, B.; Beck, W. *J. Organomet. Chem.* **1996**, *15*, 823.

(17) Neve, F.; Crispini, A. *Eur. J. Inorg. Chem.* **2000**, 1039.

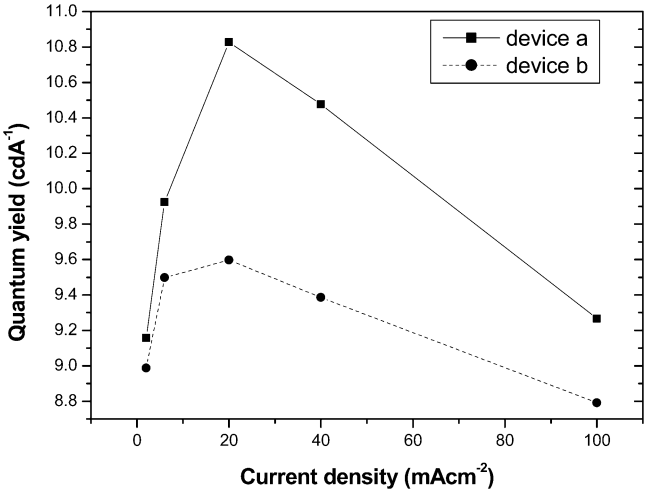

Figure 6. Plot of external quantum efficiencies (cd A^{-1}) versus current density for OLED devices using (4-CF_3bt)$_2$Ir(acac):CBP and (bt)$_2$Ir(acac):CBP as emissive layers.

Table 4. Comparative Study of the Electroluminescent Properties of the Complex-Dopants 1 and 2 Device Structure: ITO/NPB (500 Å)/CBP + 7% Dopant (200 Å)/BCP (100 Å)/Alq_3(650 Å)/LiF(10 Å)/Al(2000 Å)

	Ir(bt)$_2$(acac)	Ir(CF_3-bt)$_2$(acac)
EL color	yellow	yellow
peak wavelength	564 nm	568 nm
CIE-x	0.49	0.53
CIE-y	0.48	0.47
luminance	1900 cd/m^2 (at 20 mA/cm^2)	2166 cd/m^2 (at 20 mA/cm^2)
external quantum efficiency	7.79 (0.5 mA/cm^2) 9.50 (6 ...) 9.60 (100..)	8.12 cd/A (0.5 mA/cm^2) 9.92 (6.....) 10.83..(20...)
power efficiency (lm/W)	4.67 (at 5.18 V)	4.63 (at 5.52 V)

Furthermore, Table 4 also summarizes and compares the EL performances of device **a** against device **b**. It has been observed that the quantum efficiency of the devices **a** and **b** was found to increase with increasing current density and it shows a maximum at 10.8 and 9.6 cd/A, respectively, at 20 mA cm^{-2}. Then the efficiency starts to decrease with increasing current density for both devices as indicated in Figure 6, which can be attributed to the increasing triplet−triplet annihilation of the phosphor-bound excitons.[18−20]

The power efficiencies were found to be 4.6 and 4.7 lm/W for the devices, **a** and **b,** respectively. On the other hand, luminance (cd m^{-2}) was found to increase with increasing current density for the devices. At a current density 20 cd m^{-2} the brightness of the EL device **a** is 9267 cd m^{-2}, whereas that for the device **b** is 8791 cd m^{-2}. The lower efficiency of the (bt)$_2$Ir(acac)-based OLED relative to that of the (CF_3bt)$_2$Ir(acac)-based device may be attributed to a lower phosphorescence efficiency of the former as compared to the latter, which is evident from the solution quantum yield reported in Table 1. To investigate the effect of hole injection layer

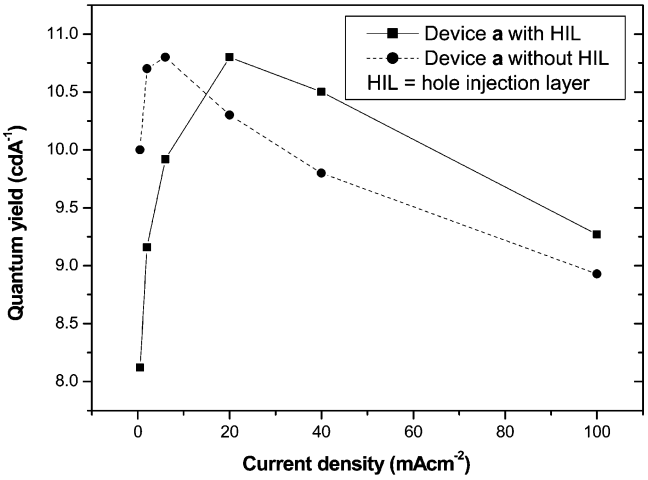

Figure 7. Plot of external quantum efficiencies (cd A^{-1}) of OLED devices using (4-CF_3bt)$_2$Ir(acac):CBP with and without hole injection layer (CHF_3).

Table 5. Comparison of Electroluminescence Properties for Device a with or without the Presence of a Hole Injection Layer (HIL)

current density mA cm^{-2}	luminance cd m^{-2}		quantum yield cd A^{-1}		power efficiency lm W^{-1}	
	with HIL	without HIL	with HIL	without HIL	with HIL	without HIL
0.50	41.4	38.4	8.28	7.69	5.53	4.67
2.00	185.9	179.8	9.29	8.99	4.97	4.38
6.00	580.1	569.8	9.67	9.50	4.31	3.91
20.00	1935.0	1920.0	9.67	9.60	3.49	3.25
40.00	3750.0	3755.0	9.37	9.39	3.00	2.85
100.00	8700.0	8791.0	8.70	8.79	2.38	2.32

on the brightness, quantum yield, and power efficiency, we have made slight modification of the device by inserting a hole injection layer, trifluoromethane, on the top of anode in each case. On comparison of the devices with a hole injecting layer with the corresponding mother devices **a** and **b,** power efficiency is always higher throughout the current densities and voltages, as indicated in Table 5 (shown only for device **a**), whereas the luminance and the quantum yield (described in Figure 7) are also found to increase at lower current densities (Table 5). These facts corroborate the good hole injecting property of trifluoromethane.

Furthermore, no emission from CBP or Alq_3 was observed, indicating a complete energy transfer from the host exciton to the Ir dopant. Meanwhile, there is no exciton decay in the Alq_3 layer due to the hole blocking action of the BCP layer. As shown in Figure 8, the device **a** having trifluoromethyl-substituted dopant shows the expected red shift and stronger intensity in the EL spectra as compared to that observed in the device **b** with unsubstituted dopant. The EL spectra of both devices match those of the same phosphors in a dilute solution. Thus, the EL emission is confirmed to originate from the triplet excited states of the phosphors. It is expected that the devices with the rest of the dopants synthesized and investigated in our work will exhibit more or less similar EL properties with the devices **a** and **b**.

Conclusions

We have synthesized a series of Ir(III) complex dopants using various types of substituted (2-phenyl)-

(18) (a) Baldo, M. A.; O'Brien, D. F.; You, Y.; Shoustikov, A.; Sibley, S.; Thompson, M. E.; Forrest, S. R. *Nature* **1998**, *395*, 151. (b) Baldo, M. A.; Lamansky, S.; Burrows, P. E.; Thompson, M. E.; Forrest, S. R. *Appl. Phys. Lett.* **1999**, *75*, 4.
(19) Baldo, M. A.; O'Brien, D. F.; Thompson, M. E.; Forrest, S. R. *Phys. Rev. B* **1999**, *60*, 14422.
(20) Adachi, C.; Baldo, M. A.; Forrest, S. R.; Thompson, M. E. *Appl. Phys. Lett.* **2000**, *78*, 170.

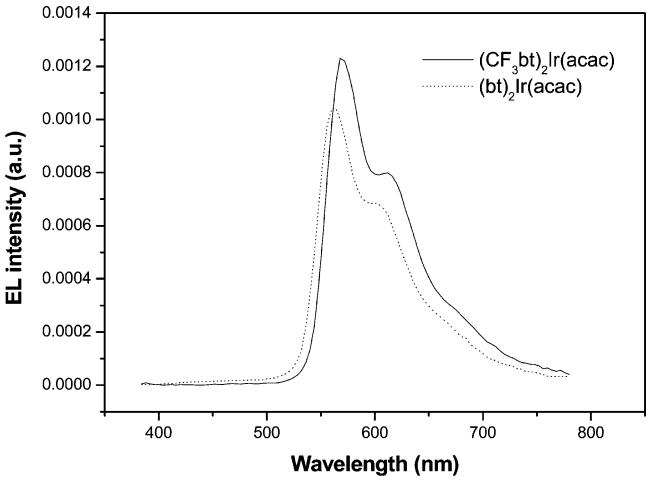

Figure 8. Plot of EL spectra of OLED devices using (4-CF_3-bt)$_2$Ir(acac):CBP and (bt)$_2$Ir(acac):CBP as emissive layers.

benzothiazole ligands. These complexes exhibit different quantum efficiencies in solution depending upon the nature of the substituents. All the complexes show one-electron oxidation in solution and the potential values are well correlated with Hammett substituent constants. The wavelength can be tuned by ∼35 nm depending upon the electronic properties of the substituents present in the ligand. Two electroluminescent devices have been fabricated and investigated and we have observed that the device with (CF_3bt)$_2$Ir(acac) as a dopant shows higher quantum efficiency and brightness as compared to that using the parent complex as a dopant.

Acknowledgment. This research is supported by the Program for Promoting University Academic Excellence from Ministry of Education, Taiwan, Republic of China, under the Contract PPAEU 91-E-FA04-2-4-(B). Professor Chin Hsin Chen and OLED Laboratory of National Chiao Tung University are gratefully acknowledged for assistance with the fabrication of OLED devices and providing helpful comments on this work.

CM030410X